PAPER

A Bayesian filtering approach to layer stripping for electrical impedance tomography

To cite this article: D Calvetti et al 2020 Inverse Problems 36 055014

View the <u>article online</u> for updates and enhancements.



IOP ebooks™

Bringing together innovative digital publishing with leading authors from the global scientific community.

Start exploring the collection-download the first chapter of every title for free.

A Bayesian filtering approach to layer stripping for electrical impedance tomography

D Calvetti[®], S Nakkireddy and E Somersalo[®]

Department of Mathematics, Applied Mathematics and Statistics, Case Western Reserve University, 10900 Euclid Avenue, Cleveland, OH 44106, United States of America

E-mail: erkki.somersalo@case.edu

Received 5 October 2019, revised 7 January 2020 Accepted for publication 24 January 2020 Published 10 April 2020



Abstract

Layer stripping is a method for solving inverse boundary value problems for elliptic PDEs, originally proposed in the literature for solving the Calderón problem of electrical impedance tomography (EIT), where the data consist of the Neumann-to-Dirichlet operator on the boundary. Defining a tangent–normal coordinate system near the boundary, the data are extended to a family of boundary operators on tangential surfaces inside the body, and it is shown that the operators satisfy a non-linear Riccati type differential equation with respect to the normal coordinate. The layer stripping process consists of a sequence of two alternating steps: the conductivity near the current boundary is estimated from the spatial high-frequency limit of the boundary data, and the boundary operator is propagated through a thin layer further into the domain via the Riccati equation. This way, the unknown conductivity in the interior of the domain is estimated layer by layer starting from the boundary and moving inward. The ill-posedness of the EIT problem manifests itself in such high sensitivity of the backwards Riccati equation to errors in the boundary data to cause the solutions to blow up in finite time, thus requiring regularization. In this article, we formulate the layer stripping process in the framework of Bayesian inverse problems, and we revisit the implementation in the light of Bayesian filtering. More specifically, we recast the related inverse boundary value problem as a state estimation problem, and propose an algorithm for its numerical solution based on ensemble Kalman filtering (EnKF). The new Bayesian layer stripping approach that we propose is quite robust, derivative-free and intrinsically suited for the quantification of uncertainties in the estimate. Furthermore, we show that the algorithm can be extended to realistic data collected by using a finite number of contact electrodes.

Keywords: ensemble Kalman filter, Grassmannian, Neumann-to-Dirichlet operator, Mobius solver, Riccati equation, modeling error

(Some figures may appear in colour only in the online journal)

1. Introduction

The goal in electrical impedance tomography (EIT) inverse problem is to reconstruct the unknown electric conductivity distribution inside a body from current-voltage measurements at the boundary. The measurements of the data can be done either by applying on the boundary a set of known electric current densities, representing the Neumann data of the governing differential equation, and measuring the resulting voltage distributions, comprising the Dirichlet data, or vice versa, by applying known voltage distributions and measuring the resulting electric current densities. Ideally, the former measurement modality would give the Neumannto-Dirichlet operator, while the latter would give its inverse, the Dirichlet-to-Neumann operator of the governing PDE. The arising EIT inverse problem, usually referred to as the Calderón problem [8], has been extensively studied in the literature [3, 32, 34, 35, 46]. The boundary operators are idealizations of the actual data, collected by attaching to the boundary of the body a finite number of contact electrodes and applying either known currents or known voltages on them, yielding the discrete counterpart of the boundary operator, the admittance matrix or the resistance matrix. The mathematical model for the electrode data is well established [16, 41], and the connection between the idealized and practical measurements, although not straightforward, is well understood [11, 23, 24].

Several numerical implementations of the Calderón problem can be found in the literature. While practical implementations usually start with the realistic electrode model, sophisticated algorithms based on idealized data have been widely studied: among them, we mention the layer stripping method [14, 15, 40, 44], the d-bar method [27], the inclusion method [26], and the sampling method [6, 7] and its generalization, the factorization method [31]. In this paper, we reformulate the layer stripping algorithm in the Bayesian framework, and leverage Bayesian filtering ideas [30] to propose a novel computational algorithm for its implementation. In addition to showing how the approach naturally provides a way to quantify the uncertainty in the computed solutions, we also outline how it can be used with realistic electrode data.

The original layer stripping algorithm was based on two basic ideas. By using a tangent–normal coordinate system near the boundary, a family of artificial boundary operators were defined on fictitious tangential boundary surfaces inside the domain. It was shown that the operator family parametrized with the normal coordinate satisfy a Riccati type operator equation, thus allowing in principle the propagation of the boundary data into the domain. However, the propagation would require the knowledge of the conductivity inside the domain. To overcome this obstacle, it was shown that the high spatial frequency asymptotics of the boundary operator determines the conductivity at the boundary surface. By extrapolating the value into a thin layer underneath the surface, the boundary data are propagated through the layer by the Riccati equation. In this way, the conductivity in the interior of the domain is estimated layer by layer, peeling the domain in an onion-like fashion. The layer stripping idea has been generalized to other PDEs [45] and systems of PDEs of elliptic type [36, 42].

Implementation of the original layer stripping algorithm poses several challenges. The continuation of the Cauchy data, and therefore the propagation of the boundary operator whose graph is the complete Cauchy data, is a highly ill-posed process that often leads to a blow-up of

the solutions. Furthermore, the conductivity reconstruction is based on high frequency asymptotics of the operators, whereas it is understood that the high frequency components deteriorate most rapidly in the propagation process. In [40], these problems were addressed by a judicious choice of the discretization scheme in the normal direction and a protocol for discarding deteriorated high frequency components while marching in. Although the viability of the method was illustrated with computed examples, the instability still remains a characteristic of the approach.

In this article, the layer stripping idea is revisited from the Bayesian point of view. Rather than propagating the boundary data inside the body, we consider a forward model in which unknown fictitious boundary data defined on an artificial boundary inside the domain are propagated outwards through a layer of unknown conductivity. The estimation of the fictitious boundary data, together with the conductivity of the layer is viewed as an inverse problem in a Bayesian setting. Moving the artificial boundary step by step deeper in the domain results in a sequence of nested inverse problems that can be recast as a Bayesian filtering problem, and using ensemble Kalman filtering (EnKF) techniques for its solution, we are able to perform the parameter estimation by a simple linear operation over an ensemble. The resulting algorithm is related to recently studied EnKF based derivative free inversion methods [13, 25, 39]. Moreover, applying similar ideas as in [1], we also incorporate the numerical approximation error of the Riccati equation in the filtering scheme. The viability of the method is illustrated by computed examples. Finally, we extend the method to the complete electrode data, bypassing the ill-posed process of approximating the continuous boundary data from true measurement data.

2. Layer stripping

We start by reviewing the ideas behind the layer stripping algorithm. For simplicity, the discussion is restricted to the case where the domain is a two-dimensional disc with unit radius, $\Omega = \{(x_1, x_2) \mid x_1^2 + x_2^2 < 1\}$, although the method can be used with general domains with C^2 -boundary provided that a tangent–normal coordinate system is available. The existence of such system for general domains can be shown by the Riemann mapping theorem.

Let $\sigma \in C^1(\overline{\Omega})$, and assume that $\sigma \geqslant \sigma_0 > 0$, for some constant σ_0 . Using the notation

$$H_0^{1/2}(\partial\Omega)=\{w\in H^{1/2}(\partial\Omega)\mid \int_{\partial\Omega}w\mathrm{d}S=0\},$$

we consider the boundary value problem

$$\nabla \cdot (\sigma \nabla u) = 0 \text{ in } \Omega \tag{1}$$

$$\sigma \frac{\partial u}{\partial n} = f \text{ on } \partial \Omega, \quad f \in H_0^{1/2}(\partial \Omega), \tag{2}$$

with the ground condition

$$\int_{\partial\Omega} u dS = 0.$$

Standard elliptic regularity results ([19], chapter 6.3.2) guarantee that the solution is in $H^2(\Omega)$. In fact, the assumptions about σ can be slightly weakened to Lipschitz continuity (see [22], theorem 3.1.3.1). Given the solution $u \in H^2(\Omega)$ of the above problem, the Neumann-to-Dirichlet operator

$$W: H_0^{1/2}(\partial\Omega) \to H^{3/2}(\partial\Omega), \quad f \mapsto [u]_{r=1},$$

defines the noiseless boundary data. The inverse problem is to estimate σ from noisy observations of W.

2.1. Propagation of the boundary data

The first step in the layer stripping algorithm consists of embedding the boundary operator W into a continuous family of operators. Let $u = u(r, \theta)$ be the solution of (1) and (2) expressed in polar coordinates. For $0 < R \le 1$, we re-parametrize u and σ restricted to a disc of radius R by defining the notations

$$u_R(t,\theta) = u(Rt,\theta), \quad \sigma_R(t,\theta) = \sigma(Rt,\theta), \quad 0 \leqslant t \leqslant 1, \quad 0 \leqslant \theta < 2\pi.$$

Defining the scaled Cartesian coordinates as

$$\xi = (\xi_1, \xi_2) = (t \cos \theta, t \sin \theta) \in \Omega,$$

it is straightforward to check that

$$\nabla_{\varepsilon} \cdot (\sigma_R \nabla_{\varepsilon} u_R) = 0 \text{ in } \Omega.$$

We define a continuous family of Neumann-to-Dirichlet operators,

$$W_R: \left[\sigma_R \frac{\partial u_R}{\partial t}\right]_{t=1} \mapsto [u_R]_{t=1}.$$

Denoting by $\langle \cdot, \cdot \rangle$ the duality between $H^s(\partial\Omega)$ and $H^{-s}(\partial\Omega)$, s > 0, extending the standard $L^2(\partial\Omega)$ inner product, we define

$$H_0^{-s}(\partial\Omega) = \{ w \in H^{-s}(\partial\Omega) \mid \langle w, 1 \rangle = 0 \}.$$

The operators W_R constitute a family of pseudo-differential operators with the smoothing property

$$W_R: H_0^s(\partial\Omega) \to H^{s+1}(\partial\Omega), -1/2 \leq s \leq 1/2.$$

The noiseless boundary data W can be identified as $W = W_1$.

Consider the complete Cauchy data

$$U_R = U_R(\theta) = \begin{bmatrix} v_R \\ w_R \end{bmatrix} \in H^{3/2}(\partial\Omega) \times H_0^{1/2}(\partial\Omega),$$

where $v_R = v_R(\theta)$ and $w_R = w_R(\theta)$ are defined as

$$v_R = [u_R]_{t=1}, \quad w_R = \left[\sigma_R \frac{\partial u_R}{\partial t}\right]_{t=1}.$$

To calculate the derivatives of these two functions with respect to R we begin by observing that $v_R(\theta) = u(R, \theta)$, and therefore

$$\dot{v}_R = \frac{\partial v_R}{\partial R} = \frac{1}{R\sigma(R,\theta)} \left[\sigma(Rt,\theta) \frac{\partial}{\partial t} u(tR,\theta) \right]_{t=1} = \frac{1}{R\sigma(R,\theta)} w_R,$$

The derivative of the second component can be computed in a similar manner, first writing

$$\dot{w}_R = \frac{\partial w_R}{\partial R} = \frac{\partial}{\partial R} \left[\sigma(R, \theta) R \frac{\partial u}{\partial R}(R, \theta) \right],$$

and, expressing the differential equation (1) in polar coordinates,

$$\dot{w}_R = -\frac{1}{R}\frac{\partial}{\partial \theta} \left[\sigma(R,\theta) \frac{\partial}{\partial \theta} u(R,\theta) \right] = -\frac{1}{R}\frac{\partial}{\partial \theta} \left[\sigma(R,\theta) \frac{\partial}{\partial \theta} v_R \right],$$

which is a well defined element of $L^2(\Omega)$ since $u \in H^2(\Omega)$.

By defining the operators

$$G_R: H_0^{1/2}(\partial\Omega) \to H^{1/2}(\partial\Omega), \quad \varphi \mapsto \frac{1}{R}\sigma(R,\cdot)^{-1}\varphi,$$

 $S_R: H_0^{1/2}(\partial\Omega) \to H^{1/2}(\partial\Omega), \quad \varphi \mapsto \frac{1}{R}\sigma(R,\cdot)\varphi,$

and

$$D: H^s(\partial\Omega) \to H^{s-1}_0(\partial\Omega), \quad \varphi \mapsto \frac{\partial \varphi}{\partial \theta}, \, s \geqslant 1/2,$$

we arrive at the identity

$$\dot{U}_R = \begin{bmatrix} \dot{v}_R \\ \dot{w}_R \end{bmatrix} = \begin{bmatrix} 0 & G_R \\ -D S_R D & 0 \end{bmatrix} U \in H^{1/2}(\partial \Omega) \times H_0^{-1/2}(\partial \Omega).$$

The mapping properties of G_R and S_R can be verified, e.g., by interpolation between $L^2(\partial\Omega)$ and $H^1(\partial\Omega)$ [4].

Differentiating both sides of the equation $W_R w_R = v_R$ with respect to R leads to

$$\dot{W}_R w_R + W_R \dot{w}_R = \dot{v}_R.$$

and after substituting the formulas for the derivatives, we obtain

$$\dot{W}_R w_R = \dot{v}_R - W_R \dot{w}_R = \frac{1}{R} (G_R w_R + W_R D S_R D v_R)$$

$$= \frac{1}{R} (G_R + W_R D S_R D W_R) w_R,$$

thus proving that the Neumann-to-Dirichlet operator satisfies the Riccati equation

$$R\frac{\mathrm{d}W_R}{\mathrm{d}R} = G_R + W_R D S_R D W_R. \tag{3}$$

The above equation can be understood as an operator equation $H_0^{1/2}(\partial\Omega) \to H^{1/2}(\partial\Omega)$. Indeed, the mapping properties of the non-linear term follow as

$$\begin{split} H_0^{1/2}(\partial\Omega) &\xrightarrow{W_R} H^{3/2}(\partial\Omega) \xrightarrow{D} H_0^{1/2}(\partial\Omega) \xrightarrow{S_R} H^{1/2}(\partial\Omega) \xrightarrow{D} H_0^{-1/2}(\partial\Omega) \\ &\xrightarrow{W_R} H^{1/2}(\partial\Omega), \end{split}$$

The Riccati equation is what makes it possible to continue the boundary data into the domain Ω , assuming that the conductivity, and therefore the operators G_R and S_R are known. The estimation of the conductivity at the boundary can be based on the high frequency asymptotics as shown below.

2.2. Boundary reconstruction

Physically, a highly oscillatory current density applied on the body surface penetrates only a small depth, and therefore the corresponding voltage density depends only on the conductivity at or near the boundary. This idea can be expressed more precisely in terms of the entries of the matrix representation of W_R in the Fourier basis of the boundary operator. The following limit result was proved in [40]: we have

$$\lim_{|k| \to \infty} |k| \langle e^{i(n+k)\theta}, W_R e^{ik\theta} \rangle = \frac{1}{2\pi R} \int e^{in\theta} \frac{1}{\sigma(R, \theta)} d\theta, \tag{4}$$

that is, the *n*th Fourier coefficient of the reciprocal of the conductivity, or resistivity, is found as a limit of the entries in the *n*th diagonal of the above infinite matrix.

2.3. Layer stripping algorithm

For completeness, we briefly summarize the original layer stripping algorithm in terms of the results above. Given the boundary operator $W = W_1$, (4) offers a way to estimate the conductivity at the outer boundary. Assuming that the conductivity does not vary rapidly in the radial direction, the boundary conductivity can be approximately extrapolated to a thin subsurface layer of thickness $\delta \ll 1$ and the boundary data W_1 can be propagated through the layer using a numerical approximation of the Riccati equation (3), yielding an approximation of $W_{1-\delta}$. At this point, one can use (4) again to find a numerical approximation for $\sigma(R - \delta, \theta)$. Continuing this process recursively, the data is propagated from the boundary to the inside of the domain Ω layer by layer, until the conductivity is approximately reconstructed in the entire domain.

Since the algorithm relies on the continuation of the Cauchy data and the high frequency asymptotics, two procedures known for their intrinsic ill-posedness, the numerical challenges that need to be overcome are significant. In [40], the regularization comprised a judicious choice of the marching steps and a scheme for discarding high frequency components when they became unreliable. Our main novel contribution to layer stripping is a different way for dealing with the inherent ill-posedness. Before presenting the new proposed algorithm, we revisit the numerical approximation of the Riccati equation.

3. Matrix approximation of the Riccati equation

In the following, we derive a finite dimensional approximation of the Riccati equation and discuss a related, computationally efficient propagation scheme.

Let n > 0 be a given even integer. Define the n trigonometric basis vectors orthonormal with respect to the $L^2(\partial\Omega)$ inner product,

$$\varphi_j(\theta) = \frac{1}{\sqrt{\pi}}\cos j\theta, \quad \varphi_{n/2+j}(\theta) = \frac{1}{\sqrt{\pi}}\sin j\theta, \quad j = 1, 2, \dots, n/2,$$

and denote by W_R , G_R , S_R , and D the matrix approximations of the operators W_R , G_R , S_R , and D respectively. More specifically, letting $H_n = \text{span}\{\varphi_j, 1 \leq j \leq n\}$, for any $f = \sum_{k=1}^n f_k \varphi_k \in H_n$,

$$\langle \varphi_j, W_R f \rangle = \sum_{i=1}^n \left[W_R \right]_{jk} f_k, \quad \left[W_R \right]_{jk} = \langle \varphi_j, W_R \varphi_k \rangle,$$

the brackets indicating the natural dual pairing. The other matrices are defined in a similar manner with expressions given below. Let R > 0 be fixed, $\sigma = \sigma(R, \theta)$ and let

 $\rho = \rho(R, \theta) = 1/\sigma(R, \theta)$ denote the resistivity for fixed radial variable R. The sine and cosine Fourier coefficients of the function ρ are denoted by

$$\rho_j^{(c)} = \frac{1}{\pi} \int_0^{2\pi} \rho(R, \theta) \cos j\theta d\theta,$$

$$\rho_j^{(s)} = \frac{1}{\pi} \int_0^{2\pi} \rho(R, \theta) \sin j\theta d\theta.$$

Then, for $f = \sum_{k=1}^{n} f_k \varphi_k \in H_n$, we have

$$\langle \varphi_j, \rho f \rangle = \sum_{j=1}^n f_k \langle \varphi_j, \rho \varphi_k \rangle = \sum_{k=1}^n [G_R]_{jk} f_k,$$

where the matrix G_R is

$$G_{R} = \left[\frac{\langle \cos j\theta, \rho \cos \ell\theta \rangle_{1 \leqslant j,k \leqslant n/2} |\langle \cos j\theta, \rho \sin k\theta \rangle_{1 \leqslant j,k \leqslant n/2}}{\langle \sin j\theta, \rho \cos k\theta \rangle_{1 \leqslant j,k \leqslant n/2} |\langle \sin j\theta, \rho \sin k\theta \rangle_{1 \leqslant j,k \leqslant n/2}} \right]$$
(5)

$$= \frac{1}{2} \left[\frac{(\rho_{j+k}^{(c)} + \gamma_{|j-k|} \rho_{|j-k|}^{(c)})_{1 \leqslant j,k \leqslant n/2}}{(\rho_{j+k}^{(s)} + \operatorname{sign}(j-k) \rho_{|j-k|}^{(s)})_{1 \leqslant j,k \leqslant n/2}} \frac{(\rho_{j+k}^{(s)} - \operatorname{sign}(j-k) \rho_{|j-k|}^{(s)})_{1 \leqslant j,k \leqslant n/2}}{(-\rho_{j+k}^{(c)} + \gamma_{|j-k|} \rho_{|j-k|}^{(c)})_{1 \leqslant j,k \leqslant n/2}} \right]$$
(6)

with $\gamma_j = 1 + \delta_{j0}$. Similarly,

$$\langle \varphi_j, \sigma f \rangle = \sum_{j=1}^n f_k \langle \varphi_j, \sigma \varphi_k \rangle = \sum_{k=1}^n [S_R]_{jk} f_k,$$

where

$$S_{R} = \left[\frac{\langle \cos j\theta, \sigma \cos \ell\theta \rangle_{1 \leqslant j,k \leqslant n/2} |\langle \cos j\theta, \sigma \sin k\theta \rangle_{1 \leqslant j,k \leqslant n/2}}{\langle \sin j\theta, \sigma \cos k\theta \rangle_{1 \leqslant j,k \leqslant n/2} |\langle \sin j\theta, \sigma \sin k\theta \rangle_{1 \leqslant j,k \leqslant n/2}} \right]$$
(7)

$$= \frac{1}{2} \left[\frac{(\sigma_{j+k}^{(c)} + \gamma_{|j-k|} \sigma_{|j-k|}^{(c)})_{1 \leqslant j,k \leqslant n/2} | (\sigma_{j+k}^{(s)} - \operatorname{sign}(j-k) \sigma_{|j-k|}^{(s)})_{1 \leqslant j,k \leqslant n/2}}{(\sigma_{j+k}^{(s)} + \operatorname{sign}(j-k) \sigma_{|j-k|}^{(s)})_{1 \leqslant j,k \leqslant n/2} | (-\sigma_{j+k}^{(c)} + \gamma_{|j-k|} \sigma_{|j-k|}^{(c)})_{1 \leqslant j,k \leqslant n/2}} \right], \quad (8)$$

where $\sigma_j^{(c)}$ and $\sigma_j^{(s)}$ denote the cosine and sine Fourier coefficients of the function $\sigma(R, \theta)$.

$$\langle \varphi_j, Df \rangle = \sum_{i=1}^n f_k \langle \varphi_j, D\varphi_k \rangle = \sum_{k=1}^n [\mathsf{D}]_{jk} f_k,$$

$$D = \begin{bmatrix} 0 & |d| \\ -d & |0| \end{bmatrix}, \tag{9}$$

where $d \in \mathbb{R}^{n/2}$ is a diagonal matrix with main diagonal entries $\{1, 2, \dots, n/2\}$.

3.1. Grassmannian flow and Möbius solver

In this subsection, we summarize our numerical solver for the Riccati equation, which is based on [38]. We begin by considering the problem in an abstract setting. Let $z = z(R) \in \mathbb{R}^{2n}$ represent the *n*th order Fourier approximation of the Cauchy data, that is,

$$z = \begin{bmatrix} z_1 \\ z_2 \end{bmatrix} = \begin{bmatrix} v \\ w \end{bmatrix}, \quad v = \begin{bmatrix} v_1 \\ \vdots \\ v_n \end{bmatrix}, \quad w = \begin{bmatrix} w_1 \\ \vdots \\ w_n \end{bmatrix},$$

with

$$v_j = \int_0^{2\pi} [u_R]_{t=1} \varphi_j d\theta, \quad w_j = \int_0^{2\pi} \left[\sigma_R \frac{\partial u_R}{\partial t} \right]_{t=1} \varphi_j d\theta.$$

Observe that we do not include the zero frequency component in v as the absolute voltage level is physically irrelevant. Consider the action of a matrix $A \in GL(2n)$ on the symplectic linear space \mathbb{R}^{2n} ,

$$z = \begin{bmatrix} z_1 \\ z_2 \end{bmatrix} \mapsto z' = \mathbf{A}z = \begin{bmatrix} \mathbf{A}_{11} & \mathbf{A}_{12} \\ \mathbf{A}_{21} & \mathbf{A}_{22} \end{bmatrix} \begin{bmatrix} z_1 \\ z_2 \end{bmatrix}.$$

If the vector components z_1 and z_2 are connected through a linear relation,

$$z_1 = \mathsf{W} z_2, \tag{10}$$

where $W = W_R$ can be identified with an element in the Grassmannian $Gr_n(2n)$, we have

$$z'_1 = A_{11}z_1 + A_{12}z_2 = (A_{11}W + A_{12})z_2$$

 $z'_2 = A_{21}z_1 + A_{22}z_2 = (A_{21}W + A_{22})z_2.$

Assuming that $(A_{21}W + A_{22})$ is invertible, we obtain a linear relation between the transformed vector components,

$$z'_1 = (A_{11}W + A_{12})(A_{21}W + A_{22})^{-1}z'_2.$$

Therefore the action of $A \in GL(2n)$ induces a non-linear transformation on $Gr_n(2n)$, given by

$$W \mapsto W' = (A_{11}W + A_{12})(A_{21}W + A_{22})^{-1}$$
.

If $z = z(R) \in \mathbb{R}^{2n}$ satisfies a linear differential equation,

$$\dot{z} = \frac{\partial z}{\partial R} = \mathbf{C}z = \begin{bmatrix} \mathbf{C}_{11} & \mathbf{C}_{12} \\ \mathbf{C}_{21} & \mathbf{C}_{22} \end{bmatrix} \begin{bmatrix} z_1 \\ z_2 \end{bmatrix},\tag{11}$$

differentiating both sides of (10), we obtain

$$\dot{z}_1 = \dot{\mathsf{W}} z_2 + \mathsf{W} \dot{z_2},$$

or

$$\dot{W}z_2 = \dot{z}_1 - W\dot{z_2}.$$

which, upon substitution yields

$$\begin{split} \dot{W}z_2 &= \dot{z}_1 - W\dot{z}_2 \\ &= C_{11}z_1 + C_{12}z_2 - W(C_{21}z_1 + C_{22}z_2) \\ &= \left(C_{11}W + C_{12} - WC_{21}W - WC_{22}\right)z_2, \end{split}$$

proving that W satisfies the Riccati equation

$$\dot{W} = C_{12} + C_{11}W - WC_{22} - WC_{21}W. \tag{12}$$

Therefore we conclude that the linear evolution model (11) in \mathbb{R}^{2n} induces a Riccati a flow (12) on the Grasmannian $Gr_n(2n)$.

Combining the two observations above yields a numerical propagation scheme of the Riccati equation. Consider the first order forward Euler scheme for (11),

$$z(R+h) \approx z(R) + C(R)z(R)h = \underbrace{(I+hC(R))}_{-A} z(R).$$

In light of the previous analysis, we define the first order propagation of $W = W_R$,

$$W_{R+h} \approx (A_{11}W_R + A_{12})(A_{21}W_R + A_{22})^{-1}$$

$$= ((I + hC_{11})W_R + hC_{12})(I + hC_{22} + hC_{21}W_R)^{-1},$$
(13)

which is well defined for |h| small enough.

For the Neumann-to-Dirichlet operator, the matrix,

$$\mathbf{C} = \mathbf{C}_R = \frac{1}{R} \begin{bmatrix} \mathbf{0} & \mathbf{G}_R \\ -\mathbf{D} \, \mathbf{S}_R \, \mathbf{D} & \mathbf{0} \end{bmatrix}$$

defines the linear evolution model for the approximate Cauchy data, hence the induced time step propagator in the Grassmannian is

$$W_{R+h} = \left(W_R + \frac{h}{R}G_R\right)\left(I - \frac{h}{R}DS_RDW_R\right)^{-1}.$$
 (14)

This propagation scheme is referred to as the first order Möbius solver. To prove the well-posedness of the propagation step for h > 0, we need the following result.

Lemma 3.1. All eigenvalues of the matrix DS_RDW_R are real and negative.

Proof. For any $\zeta \in \mathbb{C}^n$, we introduce the notation

$$f_{\zeta} = \sum_{j=1}^{n} \zeta_{j} \varphi_{j} \in H_{n},$$

where H_n has been extended to complex coefficients.

Let $\mu \in \mathbb{C}$ be an eigenvalue and $\alpha \in \mathbb{C}^n$ a corresponding eigenvector of $\mathsf{DS}_R \mathsf{DW}_R$,

$$\mathsf{DS}_R \mathsf{DW}_R \alpha = \mu \alpha.$$

Multiplying both sides from the left by $(W_R\alpha)^H$, where the superscript H indicates Hermitian transpose, we get

$$\alpha^{\mathsf{H}} \mathsf{W}_{R}^{\mathsf{T}} \mathsf{DS}_{R} \mathsf{DW}_{R} \alpha = \mu \alpha^{\mathsf{H}} \mathsf{W}_{R}^{\mathsf{T}} \alpha.$$

Since the operator W_R is symmetric positive definite (see [11]), we have

$$\alpha^{\mathsf{H}} \mathsf{W}_{R}^{\mathsf{T}} \alpha = \langle f_{\alpha}, W_{R} f_{\alpha} \rangle > 0,$$

where the duality is extended to complex vectors by taking the complex conjugate of the first term. In view of the symmetry of the matrix W_R ,

$$\alpha^{\mathsf{H}} \mathsf{W}_{R}^{\mathsf{T}} \mathsf{D} \mathsf{S}_{R} \mathsf{D} \mathsf{W}_{R} \alpha = (\mathsf{W}_{R} \alpha)^{\mathsf{H}} \mathsf{D} \mathsf{S}_{R} \mathsf{D} (\mathsf{W}_{R} \alpha),$$

and letting $\beta = W_R \alpha$, this expression can be written as

$$(\mathsf{W}_{R}\alpha)^{\mathsf{H}}\mathsf{DS}_{R}\mathsf{D}(\mathsf{W}_{R}\alpha) = \langle f_{\beta}, DS_{R}Df_{\beta} \rangle = -\langle Df_{\beta}, S_{R}Df_{\beta} \rangle$$
$$= -\int_{0}^{2\pi} \sigma(R, \theta) \left| \frac{\partial f_{\beta}(\theta)}{\partial \theta} \right|^{2} \mathrm{d}\theta < 0.$$

Therefore,

$$\mu = -\frac{\int_0^{2\pi} \sigma(R,\theta) \left| \frac{\partial f_{\beta}(\theta)}{\partial \theta} \right|^2 d\theta}{\langle f_{\alpha}, W_R f_{\alpha} \rangle} < 0,$$

thus proving the claim.

An immediate consequence of the lemma is that the propagation in the forward direction (h > 0) with (14) is well defined, whereas in the backward direction (h < 0) there is no guarantee that the spectral interval of the matrix is bounded away from the origin. Moreover, due to the roughening properties of the matrix DSDW_R , whose eigenvalues are increasing, numerical instabilities may appear already for h of small magnitude if the size of the matrix is large. However, as pointed out in [38], the singularities of the Riccati equation are coordinate singularities of the compact Grassmannian manifold, and the Möbius solver, unlike solvers based on Runge–Kutta or linear multistep methods, has no difficulties marching through them.

3.1.1. Second order scheme. For purposes of estimating the approximation error of the first order numerical scheme, a higher order method is needed. Following the ideas in [38], we first integrate the equation (11),

$$z(R+h) = z(R) + \int_0^h C(R+h_1)z(R+h_1)dh_1,$$

and by iterating, we arrive at the series representation

$$z(R+h) = z(R) + \sum_{n=1}^{\infty} \int \cdots \int_{0 \leqslant h_1 \leqslant \cdots \leqslant h_n} \mathbf{C}(R+h_n) \cdots \mathbf{C}(R+h_1) z(R) dh_1 \cdots dh_n.$$

Truncating the series at n=2 and approximating the integrals over the interval $0 \le h_1 \le h$ (n=1) and over the triangle $\{(h_1,h_2) \mid 0 \le h_2 \le h_1 \le h\}$ (n=2) by evaluating the matrix functions $\mathbb C$ at the center points of the interval, we get a second order approximation,

$$z(R+h) pprox \left(\mathsf{I} + h\mathsf{C}(R+h/2) + rac{1}{2}h^2\mathsf{C}(R+h/2)^2
ight)z(R),$$

By an argument analogous to that used for the first order Euler approximation, this linear evolution of z yields a second order accurate Möbius scheme for the matrix W. Further details concerning e.g., stiffness control, can be found in [38].

4. Layer stripping and Bayesian filtering

As pointed out above, the ill-posedness of the EIT inverse problem manifests itself as instability in the solution of the backwards Riccati equation, marching from the boundary to the interior of the domain, while solving the forward Riccati equation, i.e., marching from the inside of the domain to the boundary, is a stable process [40]. In this section, we reformulate the layer stripping as a Bayesian inverse problem and propose a numerical algorithm based on Bayesian filtering methods, and in particular, on the EnKF algorithm. In the Bayesian setting, all unknown parameters are modeled as random variables, with the belief of their values encoded in terms of probability distributions [12, 30].

Before presenting the details of the Bayesian setting, we define a suitable parametrization of the discrete problem, and derive a sequential algorithm in which the conductivity estimate is updated layer by layer inwards starting from the exterior boundary.

4.1. Parametrization

We subdivide the unit disc Ω into a finite number K of concentric annuli of radial thickness equal to the radius of the central disc. Letting h = 1/(K+1) be the radial resolution, and setting

$$1 = R_0 > R_1 > \cdots > R_K > 0, \quad R_k = 1 - kh,$$

we denote the annuli by

$$A_k = \{ (r, \theta) \mid R_k < r < R_{k-1} \}, \quad 1 \le k \le K.$$

We approximate the conductivity in each annulus by a function σ that is independent of the radial coordinate r, hence becoming a function of the angular coordinate alone, i.e.,

$$\sigma|_{A_k}(r,\theta) = \sigma_k(\theta), \quad R_k < r < R_{k-1}.$$

For each annulus A_k , $1 \le k \le K$, we define the parameter vectors $\lambda_k \in \mathbb{R}^{n_k}$,

$$(\lambda_k)_{\ell} = \log \frac{\sigma_k(\theta_{\ell})}{\sigma_0}, \quad \theta_{\ell} = \frac{\ell}{n_k} 2\pi \quad 1 \leqslant \ell \leqslant n_k,$$
 (15)

with $\lambda_{K+1} = \log \frac{\sigma(0)}{\sigma_0}$, ensuring that the estimated conductivity is strictly positive. We refer to σ_0 as the background conductivity. The value λ_{K+1} parametrizes the constant value of σ inside

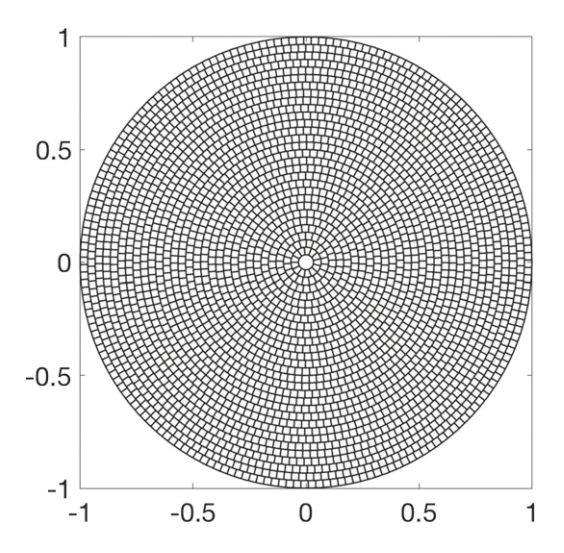


Figure 1. The discretization of the unit disc with K = 30 layers. The angular discretization is chosen so that the radial and angular discretization intervals are approximately equal.

the disc of radius R_K . To attain uniform resolution, the number n_k of discretization points in each annulus changes with its distance from the center, that is

$$n_k = \left| \frac{2\pi R_k}{h} \right|.$$

In this manner we obtain a radial pixel map of the conductivity. Figure 1 shows the discretization of the disc when K = 30.

Consider the $n \times n$ matrix approximation of the Neumann-to-Dirichlet operator on the circle of radius $r = R_k$ and introduce the notation

$$w_k \in \mathbb{R}^{n^2}$$
, $w_k = \text{vec}(\mathsf{W}_{R_k})$, $0 \leqslant k \leqslant K$,

where the operator $\operatorname{vec}: \mathbb{R}^{n \times n} \to \mathbb{R}^{n^2}$ stacks the columns of the $n \times n$ matrix into a vector of length n^2 . Observe that w_0 represents the matrix approximation of the noiseless boundary data. Furthermore, we define the aggregate vectors

$$\lambda_{(k)} = \begin{bmatrix} \lambda_1 \\ \lambda_2 \\ \vdots \\ \lambda_k \end{bmatrix} \in \mathbb{R}^{n_1 + \dots + n_k}, \quad w_{(k)} = \begin{bmatrix} w_1 \\ w_2 \\ \vdots \\ w_k \end{bmatrix} \in \mathbb{R}^{k n^2}.$$

Consider the initial value problem in the annular domain which is the union of k outmost annular A_1, \ldots, A_k ,

$$\frac{\mathrm{d}w}{\mathrm{d}R} = F(R, w, \lambda_1, \dots, \lambda_k), \quad R_k < R < 1,$$
(16)

$$w(R_k) = w_k, (17)$$

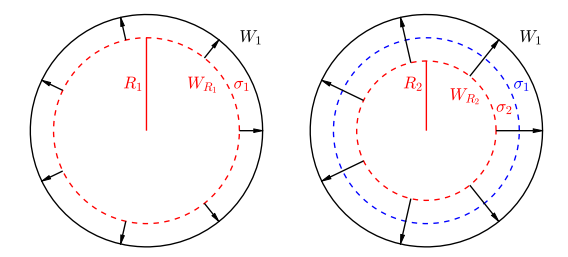


Figure 2. Schematic picture of the algorithm. The matrix $W_1 = W_{R=1}$ represents the boundary data. In the first step (left), we estimate the interior boundary value W_{R_1} and the conductivity σ_1 in the outermost ring from which we proceed to estimate the next interior boundary value W_{R_2} as well as the conductivity σ_2 . In the process, the previous estimate for σ_1 may be updated.

where F is the quadratic function in w corresponding to the Riccati equation under the current parametrization. Assume that the value of w at $R = R_0 = 1$ is observed with an additive noise, or, equivalently, that we have an observation model

$$b = w_0 + \varepsilon \in \mathbb{R}^d, \tag{18}$$

where $d=n^2$ and the random vector ε represents the noise. For the sake of definiteness, we assume that ε can be modeled as a normally distributed random variable with mean μ and covariance $\mathbf{C} \in \mathbb{R}^{d \times d}$.

4.2. Bayesian formulation

Our goal is to develop a sequential algorithm to estimate the parameter vectors λ_j , starting from the boundary and marching inside the domain. In the Bayesian paradigm, solving the inverse problem is tantamount to finding the posterior distribution that expresses the properties of the unknowns by correcting the *a priori* belief encoded in the prior distribution, in light of the contribution coming from the observations expressed via the likelihood. Before formulating the layer stripping problem in probabilistic terms, we present a brief outline of the ideas behind it.

In the spirit of the original layer stripping idea, we are looking for a sequential scheme with an updating structure of the form

$$\begin{bmatrix} w_1 \\ \lambda_{(1)} \end{bmatrix} \xrightarrow{\text{update}} \begin{bmatrix} w_2 \\ \lambda_{(2)} \end{bmatrix} \xrightarrow{\text{update}} \cdots \xrightarrow{\text{update}} \begin{bmatrix} w_K \\ \lambda_{(K)} \end{bmatrix} \to \lambda_{(K+1)}. \tag{19}$$

In other words, at each step an additional layer is added to the aggregate annular domain, and the information about the estimate of conductivity is extended to the larger domain and updated; see figure 2. The updating steps are data based, but the only available data are the outer boundary measurement b. In order to reuse the same data over and over without excessively biasing the process towards the data, we develop a Bayesian formalism similar to that used in sequential Monte Carlo (SMC) [17, 18], where the posterior density is obtained through a series of data-based updating steps of the current approximation of the posterior.

Assuming that w_k and $\lambda_1, \ldots, \lambda_k$ are known, the propagation of the initial boundary value through the annuli $A_k, A_{k-1}, \ldots, A_1$ via the Riccati equation (17), defines the forward map

$$\psi_k:(w_k,\lambda_{(k)})\mapsto w_0,$$

that does not depend on λ_{ℓ} for $\ell > k$. In this manner we define a sequence of forward observation models,

$$(\mathcal{M}_k) \quad b = \psi_k(w_k, \lambda_{(k)}) + \varepsilon_k, \quad \varepsilon_k \sim \mathcal{N}(\mu_k, \mathbf{C}_k). \tag{20}$$

To match the data with all the forward models (20), we introduce a mean likelihood model,

$$\pi_{\mathrm{lkh}}(b \mid \lambda_{(K)}, w_{(K)}) \propto \exp\left(-\frac{1}{2K} \sum_{j=1}^{K} \|b - \psi_j(w_j, \lambda_{(j)}) - \mu_k\|_{\mathsf{C}_k}^2\right)$$

$$\propto \prod_{j=1}^{K} \pi_{\mathrm{lkh}}^j(b \mid w_j, \lambda_{(j)}),$$

where

$$\pi_{\rm lkh}^j(b\mid \lambda_{(j)},w_j) \propto \exp\left(-\frac{1}{2K}\|b-\psi_j(w_j,\lambda_{(j)})-\mu_k\|_{\mathsf{C}_k}^2\right),$$

and $||z||_C^2 = z^T C^{-1}z$. In the SMC setting, this definition corresponds to writing the likelihood as a product of densities with inflated variances. Observe that the error ε_k comprises the observation error and a modeling error of the model ψ_k discussed in detail later. We remark that the mean likelihood model does not account for the correlation of the observation noise in the different models as we march inwards through the rings.

Assume that we have a sequence of prior densities,

$$\pi^1_{\text{pr}}(w_1, \lambda_1), \pi^2_{\text{pr}}(w_{(2)}, \lambda_{(2)}), \dots, \pi^K_{\text{pr}}(w_{(K)}, \lambda_{(K)});$$

using Bayes' formula, we define the kth posterior density for $(w_{(k)}, \lambda_{(k)})$ by

$$\pi_{\text{post}}^{k}(w_{(k)}, \lambda_{(k)} \mid b) \propto \pi_{\text{pr}}^{k}(w_{(k)}, \lambda_{(k)}) \prod_{i=1}^{k} \pi_{\text{lkh}}^{i}(b \mid \lambda_{(j)}, w_{j}). \tag{21}$$

The solution of our problem is the posterior density for k = K, and we construct it through a sequential process. To this end, consider first the sequence of priors. For the priors to be mutually compatible, we write

$$\pi_{\mathrm{pr}}^{k+1}(w_{(k+1)},\lambda_{(k+1)}) = \pi^{k+1}(w_{k+1},\lambda_{k+1} \mid w_{(k)},\lambda_{(k)})\pi_{\mathrm{pr}}^{k}(w_{(k)},\lambda_{(k)}),$$

and by assuming that a priori,

- (a) w_{k+1} is independent of $w_{(k)}$ and $\lambda_{(k+1)}$,
- (b) λ_{k+1} is independent of $w_{(k)}$ but not necessarily of $\lambda_{(k)}$,

the formula simplifies to

$$\pi_{\text{pr}}^{k+1}(w_{(k+1)}, \lambda_{(k+1)}) = \pi_w^{k+1}(w_{k+1})\pi_\lambda^{k+1}(\lambda_{k+1} \mid \lambda_{(k)})\pi_{\text{pr}}^k(w_{(k)}, \lambda_{(k)}), \tag{22}$$

where the densities π_w^{k+1} and π_λ^{k+1} will be specified later. According to (a), the NtD matrix on the inner surface depends only on the conductivity inside the disc but not on the outside conductivity distribution or on the NtD matrix on the surface of the outer layer. This simplifying assumption ignores the interdependencies of the inside and outside conductivity values coming from the smoothness assumption, which are explicitly taken into account by assumption (b), where the dependency of λ_{k+1} on $\lambda_{(k)}$ accounts for the smoothness assumptions on σ . The independence of λ_{k+1} and $w_{(k)}$ is a simplifying assumption to keep the algorithm tractable.

To update the posterior, we substitute the updated prior (22) in (21),

$$\pi_{\text{post}}^{k+1}(w_{(k+1)}, \lambda_{(k+1)} \mid b) \propto \pi_{\text{pr}}^{k+1}(w_{(k+1)}, \lambda_{(k+1)}) \prod_{j=1}^{k+1} \pi_{\text{lkh}}^{j}(b \mid \lambda_{(j)}, w_{j})$$

$$= \pi_{w}^{k+1}(w_{k+1}) \pi_{\lambda}^{k+1}(\lambda_{k+1} \mid \lambda_{(k)}) \pi_{\text{pr}}^{k}(w_{(k)}, \lambda_{(k)})$$

$$\times \prod_{j=1}^{k+1} \pi_{\text{lkh}}^{j}(b \mid \lambda_{(j)}, w_{j}),$$

and rewrite it as

$$\pi_{\text{post}}^{k+1}(w_{(k+1)}, \lambda_{(k+1)} \mid b) \propto \pi_w^{k+1}(w_{k+1}) \pi_\lambda^{k+1}(\lambda_{k+1} \mid \lambda_{(k)}) \pi_{\text{lkh}}^{k+1}(b \mid \lambda_{(k+1)}, w_{k+1}) \times \pi_{\text{post}}^k(w_{(k)}, \lambda_{(k)} \mid b).$$

Since we are primarily interested in the conductivity values inside Ω , we marginalize the density with respect to w_i 's and arrive at the marginalized posterior

$$\overline{\pi}_{\text{post}}^{k+1}(\lambda_{(k+1)} \mid b) = \pi_{\lambda}^{k+1}(\lambda_{k+1} \mid \lambda_{(k)}) \overline{\pi}_{\text{post}}^{k}(\lambda_{(k)} \mid b)
\times \left(\int \pi_{w}^{k+1}(w_{k+1}) \pi_{\text{lkh}}^{k+1}(b \mid \lambda_{(k+1)}, w_{k+1}) dw_{k+1} \right),$$
(23)

where

$$\overline{\pi}_{\mathrm{post}}^{k}(\lambda_{(k)} \mid b) = \int \pi_{\mathrm{post}}^{k}(w_{(k)}, \lambda_{(k)} \mid b) \mathrm{d}w_{(k)}.$$

Formula (23) is the basis for the sequential estimation of the conductivity from boundary data. It is important to observe that

- (a) the posterior density of the previous round constitutes part of the prior for the next update, in particular for the parameters $\lambda_{(k)}$,
- (b) the likelihood π_{lkh}^{k+1} concerns only the model (\mathcal{M}_{k+1}) , with the noise covariance inflated by a factor K to avoid overconfidence in the data.
- (c) the marginalized estimate of the boundary data w_k , in the particle approximation procedure that we introduce next, can be obtained by simply discarding the components to be integrated out.

The conductivity λ_{K+1} in the last layer, which is a disc, can be estimated from w_K , as it corresponds to the boundary operator of a constant conductivity disc.

4.3. Sequential estimation by EnKF

The formula (23) provides the means to update the current information about the conductivity. A natural way to explore the densities as our domain keeps growing from the boundary towards the interior of the unit disc, one annulus at a time, is to use particle methods. Our method of choice here is ensemble Kalman filtering (EnKF), which is briefly reviewed below for completeness [20, 28, 33].

Assume that we have a sequence x_0, x_1, x_2, \ldots of random variables with a stochastic propagation model $x_k \mapsto x_{k+1}$ which is tantamount to the existence of a conditional density $\pi(x_{k+1} \mid x_k)$, and a noisy observation model, where the noise is assumed to be Gaussian,

$$b_k = g_k(x_k) + \varepsilon_k, \quad \varepsilon_k \sim \mathcal{N}(\nu_k, \Sigma_k),$$

defining a likelihood density $\pi(b_k \mid x_k)$.

A single updating step of the EnKF can be summarized as follows.

(a) Propagation step: given a sample

$$\{x_k^{(1)}, x_k^{(2)}, \dots, x_k^{(N)}\}\$$

with equal weights from the current density $\pi_k(x_k)$, generate a predictive sample using the propagation model,

$$\{\widehat{x}_{k+1}^{(1)}, \widehat{x}_{k+1}^{(2)}, \dots, \widehat{x}_{k+1}^{(N)}\}, \quad \widehat{x}_{k+1}^{(j)} \sim \pi(x_{k+1} \mid x_k^{(j)}).$$

(b) Calculate the empirical mean \overline{x}_{k+1} and covariance G_{k+1} of the predictive sample

$$\overline{x}_{k+1} = \frac{1}{N} \sum_{\ell=1}^{N} \widehat{x}_{k+1}^{(\ell)}, \quad \mathsf{G}_{k+1} = \frac{1}{N} \sum_{\ell=1}^{N} \left(\widehat{x}_{k+1}^{(\ell)} - \overline{x}_{k+1} \right) \left(\widehat{x}_{k+1}^{(\ell)} - \overline{x}_{k+1} \right)^{\mathsf{T}},$$

(c) Given the observation b_{k+1} , generate a data ensemble

$$\left\{b_{k+1}^{(1)},b_{k+1}^{(2)},\ldots,b_{k+1}^{(N)}\right\},\quad b_{k+1}^{(\ell)}=b_{k+1}+\mathrm{e}_{k+1}^{(\ell)}-
u_{k+1},\quad \mathrm{e}_{k+1}^{(\ell)}\sim\mathcal{N}(0,\Sigma_{k+1}).$$

(d) Analysis step: generate a sample from the posterior by solving the set of optimization problems

$$x_{k+1}^{(j)} = \operatorname{argmin} \left\{ \|x - \widehat{x}_{k+1}^{(j)}\|_{\mathsf{G}_{k+1}}^2 + \|g_{k+1}(x) - b_{k+1}^{(j)}\|_{\Sigma_{k+1}}^2 \right\}.$$

It is well known that if the prior distribution of x^k and the distribution of x^{k+1} conditional on x^k are Gaussian and the observation model is linear, the above scheme produces a sample that is distributed according to the Gaussian posterior density. For non-Gaussian models, the sample distribution is only approximate. For a further discussion of the use of EnKF in the inverse problems, see, e.g., [25, 39].

To set up the conductivity estimation problem in the EnKF framework, we start by defining the state variables x_k as

$$x_k = \begin{bmatrix} w_0 \\ w_k \\ \lambda_{(k)} \end{bmatrix},$$

as well as the observation model,

$$b_k = \mathsf{B}_k x_k + \varepsilon_k, \quad \varepsilon_k \sim \mathcal{N}(\nu, K\Sigma),$$

where Σ is the covariance matrix of the observation noise, K the number of the annuli, inflating the noise covariance to compensate for the reuse of the data, and

$$\mathsf{B}_k = egin{bmatrix} \mathsf{I}_{n^2} & \mathsf{O}_{n^2 \times n^2} & \mathsf{O}_{n^2 \times N_{k+1}} \end{bmatrix} : x_k \mapsto w_0,$$

where I_{n^2} is the $n^2 \times n^2$ identity matrix, $O_{p \times q}$ is a null matrix of the indicated size, and $N_{k+1} = n_1 + n_2 + \cdots + n_{k+1}$. For the filtering algorithm, we need to define the stochastic evolution model. The evolution is composed by two steps,

$$x_{k} = \begin{bmatrix} w_{0} \\ w_{k} \\ \lambda_{(k)} \end{bmatrix} \xrightarrow{(a)} \begin{bmatrix} w_{k+1} \\ \lambda_{(k+1)} \end{bmatrix} \xrightarrow{(b)} \begin{bmatrix} w_{0} \\ w_{k+1} \\ \lambda_{(k+1)} \end{bmatrix} = x_{k+1},$$

where the two steps are defined as follows.

Step (a): given the current $\lambda_{(k)}$, draw λ_{k+1} from the conditional prior distribution $\pi_{\lambda}^{k+1}(\lambda_{k+1} \mid \lambda_{(k)})$, and draw w_{k+1} from the prior distribution $\pi_{w}^{k+1}(w_{k+1})$.

Step (b): propagate w_{k+1} through the k+1 layers using the first order Möbius propagator (14). Add innovation with variance estimated from the second order Möbius propagator to get w_0 .

We recall that, as in [1], the innovation term in step (b) models the unknown numerical approximation error of the first order method for the propagation. Following a standard practice in numerical time integration error control, a second order method is used to assess its size. The computational details will be explained in the following section, prior to demonstrating the viability of the algorithm with a few computed examples.

4.4. Extension to electrode model

The discussion so far has been limited to idealized Neumann-to-Dirichlet data, while in reality, the boundary measurements are carried out by attaching a finite number of contact electrodes to inject electric currents in the body and measuring the corresponding voltages at the electrodes. Let $e_\ell \subset \partial \Omega$ be non-overlapping intervals representing the electrodes, $1 \leq \ell \leq L$, and let $J \in \mathbb{R}^L$ be a current pattern, the ℓ th component J_ℓ being the current injected through e_ℓ and satisfying Kirchhoff's law arising from the conservation of charge, $\sum_{\ell=1}^L J_\ell = 0$. The complete electrode model for the EIT problem is characterized by the replacement of the Neumann condition (2) by the non-standard electrode boundary conditions,

$$\begin{split} \int_{e_\ell} \sigma \frac{\partial u}{\partial n} \mathrm{d}S &= J_\ell, \\ \sigma \frac{\partial u}{\partial n} &= 0 \quad \text{in } \partial \Omega \backslash \cup_{\ell=1}^L e_\ell, \\ \left(u + z_\ell \sigma \frac{\partial u}{\partial n} \right) \mid_{e_\ell} &= V_\ell = \text{constant}, \end{split}$$

where $z_{\ell} > 0$ is the contact impedance of the ℓ th electrode, and V_{ℓ} is the electrode voltage, the vector $V \in \mathbb{R}^L$ being the corresponding voltage pattern that needs to be solved together with u when J is given. The resistance matrix $\mathsf{R} \in \mathbb{R}^{L \times L}$ is defined through Ohm's law,

$$V = RI$$
.

The EIT problem based on electrode measurements is to estimate the conductivity from the knowledge of the matrix R. For a detailed description of the complete electrode model, we refer to [41].

In [11], the connection between the Dirichlet-to-Neumann map and the resistance map was analyzed. Let L denote the infinite matrix of the Dirichlet-to-Neumann map with respect to the

orthonormal trigonometric basis in $H^{1/2}(\partial\Omega)$,

$$\phi_0(\theta) = \frac{1}{\sqrt{2\pi}}, \quad \phi_{2j}(\theta) = \frac{1}{\sqrt{\pi j}}\cos j\theta, \quad \phi_{2j-1}\theta = \frac{1}{\sqrt{\pi j}}\sin j\theta, \quad j = 1, 2, \dots,$$
 (24)

that is,

$$(\mathsf{L})_{ik} = \langle \phi_i, \Lambda \phi_k \rangle, \quad \Lambda = W^{-1} : H^{1/2}(\partial \Omega) \to H^{-1/2}(\partial \Omega).$$

We introduce the diagonal matrix D with entries

$$\mathsf{D}_{\ell\ell} = rac{|e_\ell|}{z_\ell}, \quad 1 \leqslant \ell \leqslant L,$$

where $|e_{\ell}|$ is the size of the electrode e_{ℓ} , a matrix Y with entries

$$\mathsf{Y}_{j\ell} = rac{1}{|e_\ell|} \int_{e_\ell} \phi_j \mathrm{d}S, \quad 1 \leqslant \ell \leqslant L, \quad 0 \leqslant j < \infty,$$

and a matrix M with entries

$$\mathsf{M}_{jk} = \sum_{\ell=1}^{L} \frac{1}{z_{\ell}} \int_{e_{\ell}} \phi_{j} \phi_{k} \mathrm{d}S, \quad 0 \leqslant j, k < \infty.$$

Furthermore, let $\phi \in \mathbb{R}^{L \times (L-1)}$ denote a matrix whose columns contain the trigonometric current patterns

$$\left(\Phi_{m}\right)_{\ell} = \sqrt{\frac{(2-\delta_{m,L/2})}{L}}\cos\frac{2\pi}{L}m(\ell-1), \quad 1\leqslant \ell\leqslant L,$$

for $1 \leq m \leq L/2$, and

$$\left(\phi_{L/2+m}\right)_{\ell} = \sqrt{\frac{2}{L}}\sin\frac{2\pi}{L}m(\ell-1), \quad 1 \leqslant \ell \leqslant L,$$

for $1 \le m \le L/2 - 1$. With these notations, the following connection between the discrete and continuous boundary data can be established.

Theorem 4.1. The matrices $L: \ell^2 \to \ell^2$ and $R \in \mathbb{R}^{L \times L}$ satisfy the identity

$$\Phi^{\mathsf{T}} \mathsf{D} \Phi - (\mathsf{Y} \mathsf{D} \Phi)^{\mathsf{T}} (\mathsf{L} + \mathsf{M})^{-1} \mathsf{Y} \mathsf{D} \Phi = \widetilde{\mathsf{R}}^{-1}, \tag{25}$$

where \widehat{R} is the representation of the resistance map in the basis Φ ,

$$\widetilde{\mathsf{R}} = \Phi^\mathsf{T} \mathsf{R} \Phi \in \mathbb{R}^{(L-1) \times (L-1)}$$
.

For the proof, see theorem 3.3 of [11].

In particular, from the analysis in [11] it follows that if a finite matrix approximation of the operator W is given, we can estimate in a stable way the resistance matrix based on the above formula, while the converse is an ill-posed problem. This observation allows us to extend the Bayesian layer stripping algorithm to electrode data. Indeed, the above theorem defines a mapping

$$F: \mathbb{R}^{n^2} \to \mathbb{R}^{(L-1)^2}, \quad w_0 \mapsto r = \text{vec}(\widetilde{R}).$$
 (26)

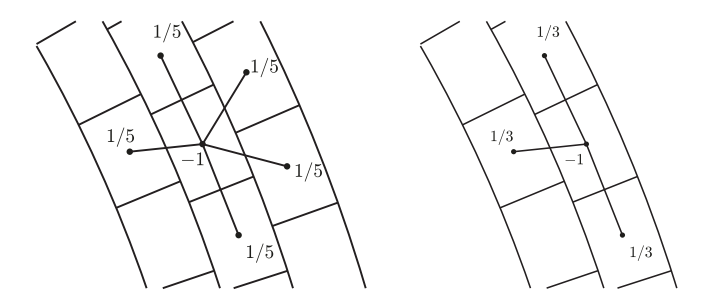


Figure 3. The discrete approximation of the Laplacian uses a six point stencil for pixel centers not in the outermost layer (left) and a four point stencil for points in the outermost layer (right). The coefficients are indicated in the figure, guaranteeing that the discrete Laplacian satisfies the mean value principle.

Hence, if the data comprise a noisy observation of the matrix \widetilde{R} , the Bayesian filtering algorithm can be modified for electrode data by defining the particles as

$$x_k = \begin{bmatrix} F(w_0) \\ w_k \\ \lambda_{(k)} \end{bmatrix},$$

while keeping everything else in the algorithm intact.

5. Computational details

In this section we present the details of the implementation of the EnKF layer stripping algorithm. We start by discussing the prior models that constitute the first step in the particle propagation, then comment on how to address modeling errors due to numerical approximations that may affect the results.

5.1. Prior densities

The first step in the particle propagation scheme requires priors for generating the log-conductivity in the next ring when marching inwards, as well as a generation of a new random initial value of the Neumann-to-Dirichlet map at the new interior boundary.

5.1.1. Conditional priors for log-conductivity. Consider first the problem of drawing λ_{k+1} given $\lambda_{(k)}$. To define the process of generating random samples conditional on estimated values in the exterior rings, we denote by $\{p_k\}$ the set of pixel centers, augmented with the center of the disc Ω . We denote by L a discrete graph Laplacian computed over the vertices p_k . We use a six point stencil of five nearest neighbor pixels to approximate the Laplacian in pixels that are not in the outermost layer, and a four point stencil in the outer ring, as explained graphically in figure 3.

Consider now the vector $\lambda_{(K+1)}$, partitioned as

$$\lambda_{(K+1)} = \begin{bmatrix} \lambda_{(k)} \\ \lambda_{k+1} \\ \vdots \\ \lambda_{K+1} \end{bmatrix} = \begin{bmatrix} \lambda_{(k)} \\ \lambda'_{(k)} \end{bmatrix}, \quad \lambda'_{(k)} = \begin{bmatrix} \lambda_{k+1} \\ \vdots \\ \lambda_{K+1} \end{bmatrix},$$

and partition the matrix L accordingly,

$$\mathsf{L} = \begin{bmatrix} \mathsf{L}_{(k)} & \mathsf{L}'_{(k)} \end{bmatrix},$$

Postulating that $\lambda_{(K+1)}$ follows a second order smoothness prior, $\alpha L \lambda_{(K+1)} \sim \mathcal{N}(0, I)$, for some scaling parameter α , the joint probability density of $\lambda_{(k)}$ and $\lambda_{(k)}'$ can be written as

$$\begin{split} \pi(\lambda_{(K+1)}) &= \pi(\lambda_{(k)}, \lambda'_{(k)}) \propto \exp\left(-\frac{\alpha^2}{2} \|\mathsf{L}\lambda_{(K+1)}\|^2\right) \\ &= \exp\left(-\frac{\alpha^2}{2} \|\mathsf{L}_{(k)}\lambda_{(k)} + \mathsf{L}'_{(k)}\lambda'_{(k)}\|^2\right). \end{split}$$

Introducing the matrix

$$B = L^T L = \begin{bmatrix} B_{11} & B_{12} \\ B_{21} & B_{22} \end{bmatrix},$$

where

$$\mathsf{B}_{11} = \mathsf{L}_{(k)}^\mathsf{T} \mathsf{L}_{(k)}, \quad \mathsf{B}_{22} = (\mathsf{L}_{(k)}')^\mathsf{T} \mathsf{L}_{(k)}', \quad \text{and} \quad \mathsf{B}_{12} = \mathsf{L}_{(k)}^\mathsf{T} \mathsf{L}_{(k)}' = \mathsf{B}_{21}^\mathsf{T},$$

the probability density of $\lambda'_{(k)}$ conditional on $\lambda_{(k)}$ can be expressed as

$$\pi\left(\lambda'_{(k)}|\lambda_{(k)}\right) \propto \exp\left(-\frac{\alpha^2}{2}(\lambda'_{(k)} + \mathsf{B}_{22}^{-1}\mathsf{B}_{21}\lambda_{(k)})^\mathsf{T}\mathsf{B}_{22}(\lambda'_{(k)} + \mathsf{B}_{22}^{-1}\mathsf{B}_{21}\lambda_{(k)})\right). \tag{27}$$

Since the matrix $L'_{(k)}$ is of full rank, B_{22} is invertible, and we can draw random samples of $\lambda'_{(k)}$ conditional on $\lambda_{(k)}$ from the normal distribution $\mathcal{N}(-B_{22}^{-1}B_{21}\lambda_{(k)},\frac{1}{\alpha^2}B_{22}^{-1})$. The conditional density $\pi_{\lambda}^{k+1}(\lambda_{k+1} \mid \lambda_{(k)})$ used for the updating scheme is obtained by marginalizing over the components $\lambda_{k+2},\ldots,\lambda_{K+1}$, which in practice is done by simply discarding the components from $\lambda'_{(k)}$.

To complete the discussion, we need a prior model to initialize the process by drawing the log-conductivities λ_1 in the outermost layer.

To do this, we introduce a periodic discrete Laplacian L_1 , defined over the pixel centers of the outermost layer by

$$\mathsf{L}_1 = \begin{bmatrix} -2 & 1 & 0 & \cdots & 1 \\ 1 & -2 & 1 & & 0 \\ & \ddots & \ddots & \ddots & \\ & & 1 & -2 & 1 \\ 1 & 0 & \cdots & 1 & -2 \end{bmatrix} \in \mathbb{R}^{n_1},$$

and define a Whittle–Matérn prior with correlation length $\ell_1 > 0$,

$$\lambda_1 \sim \mathcal{N}(0, \Xi_1), \quad \Xi_1^{-1} = \frac{1}{\alpha_1^2} (-\mathsf{L}_1 + \ell_1^{-2} \mathsf{I}_{n_1})^\mathsf{T} (-\mathsf{L}_1 + \ell_1^{-2} \mathsf{I}_{n_1}).$$

where $\alpha_1 > 0$ is a scaling parameter [37]. The choice of the scaling parameters α and α_1 and of the correlation length ℓ_1 is discussed in the section in the context of the computed examples.

5.1.2. Prior model for the interior boundary values. We define next the process to generate the sample of the Neumann-to-Dirichlet data in the inner boundary at $R = R_k$ of the annulus. For simplicity, we generate a sample of radially symmetric conductivity profiles and compute the corresponding Neumann-to-Dirichlet matrices. To generate radial log-conductivity profiles that are not too oscillatory, we define a second order finite difference matrix

$$\mathsf{L}_{A} = rac{1}{h^{2}} egin{bmatrix} -\delta & & & & & & & \\ 1 & -2 & 1 & & & & & \\ & \ddots & \ddots & \ddots & & & \\ & & 1 & -2 & 1 & & \\ & & & & -\delta \end{bmatrix} \in \mathbb{R}^{K+1},$$

where $\delta > 0$ is a parameter controlling the variance of the end values, see [12] for a criterion of choice, and define the Whittle–Matérn covariance matrix [37] for a radial correlation length $\ell_r > 0$,

$$\Xi_{\mathbf{r}}^{-1} = \frac{1}{\alpha_{\mathbf{r}}^{2}} (-\mathsf{L}_{A} + \ell_{\mathbf{r}}^{-2} \mathsf{I}_{n_{k}})^{\mathsf{T}} (-\mathsf{L}_{A} + \ell_{\mathbf{r}}^{-2} \mathsf{I}_{n_{k}}),$$

and generate a random log-conductivity profile $\lambda \sim \mathcal{N}(0,\Xi_r)$ from which we computed the conductivity profile $\sigma \in \mathbb{R}^{K+1}$ according to (15).

For each random realization of the conductivity profile, we compute the diagonal entries of the Neumann-to-Dirichlet matrix, using the exact propagation formula for a piecewise constant conductivity model derived in [40]. More specifically, given a piecewise constant conductivity profile $\sigma = [\sigma_1, \ldots, \sigma_{K+1}]$,

(a) Set

$$w_j(R_K) = \frac{1}{j\sigma_{K+1}}, \quad 1 \leqslant j \leqslant j_{\text{max}},$$

(b) Propagate w_i through the rings $R_k < R < R_{k-1}$ by the formula

$$w_j(R_{k-1}) = \frac{1}{j\sigma_k} M\left(\left[\frac{R_k}{R_{k-1}}\right]^{2j} M\left(j\sigma_k w_j(R_k)\right)\right),\tag{28}$$

where
$$M(t) = (1 - t)/(1 + t)$$
.

The radial symmetry in the sample construction is a limitation assumed for computational convenience, however numerical experiments show that it does not seem to bias significantly the results of the inverse towards radially symmetric solutions.

5.2. Approximation error in the propagator

A natural question arising when particle methods, e.g., the EnKF, are applied to deterministic models, is how to assign the innovation term in the propagation step. One possibility, advocated e.g., in [1], is to interpret the stochastic innovation as an expression of the uncertainty in the numerical approximation of the deterministic propagation model. This interpretation is particularly useful for parallel implementation of the methods. To set the variance of the innovation, it is necessary to have an estimate of the numerical error, which can be obtained by pairing the method of choice with a higher order method that in this case is the second order Möbius solver [38].

5.3. Data, noise model and approximation error in the forward solver

We test the viability of the algorithm in the two-dimensional case by generating the synthetic boundary data with a second order finite element model. To improve the accuracy of the solution at the boundary where the data are collected, isoparametric elements with second order shape functions are employed [5, 21]. We assume here that the finite element mesh is chosen fine enough for the FEM model to produce an accurate approximation of the noiseless data. The details are discussed further in the section on computed examples.

When testing the robustness of an algorithm with respect to observation noise, one cannot ignore the modeling error contribution, which, in the current application, is coming from the discrepancy between the data generated by the FEM code that approximates the noiseless observations and the model predictions obtained by the forward model used in the inverse solver, which in the current version is the Riccati equation approximated by the Möbius solver. It has been demonstrated [2, 9, 10, 29, 30] that when the exogenous noise level in the data is low, ignoring the modeling error may have adverse effects on results: a too optimistic likelihood model forces the estimates to explain the modeling error by fictitious conductivity structures inside the object, and since the problem is ill-posed, the induced artifacts may be significantly strong. Furthermore, it has been demonstrated that often the modeling error has non-vanishing mean and structured covariance. Therefore, to account for the modeling error, we perform the following analysis. Consider the model (\mathcal{M}_k) , equation (20), and assume that the model ψ^* represents accurately the noiseless data. If ε^* denotes the exogenous noise, we can write

$$b = \psi^*(\lambda_{(K+1)}) + \varepsilon^*$$

= $\psi_k(w_k, \lambda_{(k)}) + \left[\psi^*(\lambda_{(K+1)}) - \psi_k(w_k, \lambda_{(k)})\right] + \varepsilon^*,$

where the term inside the square brackets represents the modeling error. This suggests that the noise term ε in (20) should account for both the modeling error and the exogenous error. Since the modeling error depends on the unknown, it has been proposed in the literature to use a Gaussian approximation, with mean and covariance computed from a sample of realizations corresponding to conductivities drawn from the prior [2, 29, 30]. Further improvements of the approximation using iterative updating were considered in [9, 10].

Rather than estimating the modeling error corresponding to ψ_k for each k, we perform the analysis only once with k=K and use the same estimated modeling error mean and covariance for all k. First, we draw a sample $\{\lambda^1,\ldots,\lambda^M\}$ of smooth log-conductivities, compute the corresponding conductivities, and generate the boundary data in two different ways: Using the second order FEM model ψ^* that in our simulations represents accurately the measurement process, and by evaluating the functions λ^ℓ at the pixel centers to get the vectors $\lambda^\ell_{(K+1)}$ and using the Riccati solver $\psi_K(w_K^\ell,\lambda_{(K)}^\ell)$ that is the forward model in our algorithm. Denoting the data samples by $\{m_j^1,m_j^2,\ldots,m_j^M\}$, where j=1 corresponds to the FEM model and j=2 to the Riccati model, we compute the modeling error sample,

$$\varepsilon_{\text{mod}}^k = m_1^k - m_2^k, \quad 1 \leqslant k \leqslant M,$$

and estimate its the mean and covariance as

$$\mu = \frac{1}{M} \sum_{k=1}^{M} \varepsilon_{\text{mod}}^{k}, \quad \mathsf{C}_{\text{mod}} = \frac{1}{M} \sum_{k=1}^{M} (\varepsilon_{\text{mod}}^{k} - \mu) (\varepsilon_{\text{mod}}^{k} - \mu)^{\mathsf{T}}.$$

The approximate noise model comprising both the exogenous and modeling noise is

$$\varepsilon = \varepsilon_{\text{mod}} + \varepsilon_{\text{ex}} \sim \mathcal{N}(\mu, C_{\text{mod}} + C_{\text{ex}}),$$

Table 1. Parameter values used in the algorithm.

K	Number of layers	30
n	Number of Fourier modes	60
N	Ensemble size	1000
L	Number of electrodes	32

Table 2. Parameter values used for defining the prior densities.

σ_0	Background conductivity	1.5
α	Prior scaling for $\lambda_{(K+1)}$	0.01
α_1	Prior scaling at outer ring	0.004
ℓ_1	Correlation length at outer ring	10
δ	Boundary variance in L_A	0.0768
$\alpha_{\rm r}$	Prior scaling for radially symmetric sample	0.2
$\ell_{\rm r}$	Radial correlation length	2
Γ	Innovation in the radial AR(2) model	0.08

Table 3. Parameter values defining the noise level, including those used for estimating the approximation error.

η_1	Noise level relative to $ b _{\infty}$, radial model	$\sqrt{10^{-3}}$
η_2	Noise level relative to $ b _{\infty}$, non-radial model	$\sqrt{10^{-7}}$
M	Sample size of modeling error realizations	1000

where C_{ex} is the covariance matrix of the exogenous noise that we assume to have vanishing mean.

6. Computed examples

We demonstrate the viability of the proposed algorithm with computed examples. As a proof of concept, we test the method with a radially symmetric profile, and subsequently with a more realistic non-symmetric problem. In the non radially symmetric case, we consider both the Neumann-to-Dirichlet data as well as the electrode data. The number of Fourier modes included, number of electrodes and number of layers in the model are given in table 1. The parameters defining the prior densities as well as the noise simulations are listed in tables 2 and 3.

6.1. Radial conductivities

We consider first the case in which the conductivity is radially symmetric, and the inverse problem is to estimate the radial profile from the diagonal entries of the Neumann-to-Dirichlet map. Because of the radial symmetry, the entries corresponding to sine and cosine current patterns coincide, $W_{k,k} = W_{n/2+k,n/2+k}$, and the Riccati equations for the diagonal entries decouple, yielding

$$R\frac{\mathrm{d}W_{k,k}}{\mathrm{d}R} = \frac{1}{\sigma} - k^2 \sigma W_{k,k}^2, \quad 1 \leqslant k \leqslant \frac{n}{2}, \, \sigma = \sigma(R). \tag{29}$$

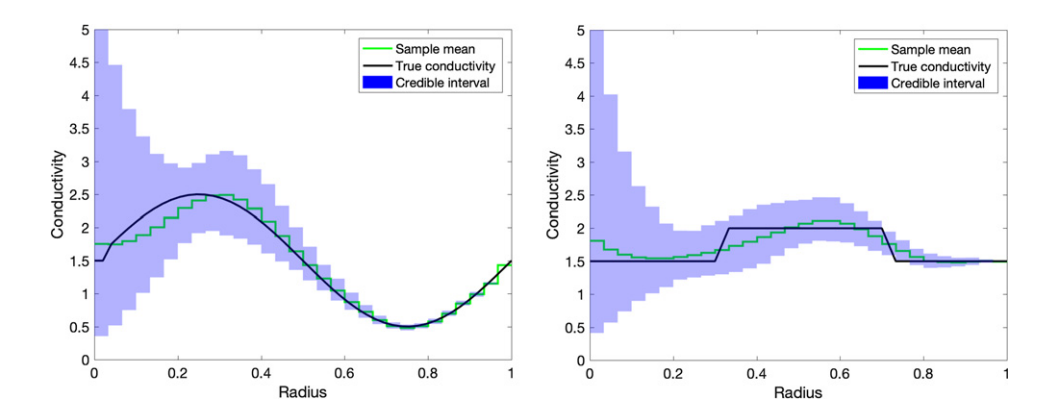


Figure 4. Reconstructions of a smooth radial conductivity profile (left) and a boxcar profile (right), including the 95% credibility envelopes.

In order to avoid the inverse crime, instead of a Möbius solver, we synthesize the data by solving (29) using Matlab built-in function ode45. In the EnKF algorithm, we approximate the conductivity by a piecewise constant function and propagate the solution according to (28). For the prediction of λ_{k+1} conditional on $\lambda_{(k)}$, in this simplified setting we use an AR(2) model based on a second order smoothness prior, that is, λ_{k+1} is drawn as

$$\lambda_{k+1} = 2\lambda_k - \lambda_{k-1} + \gamma \nu, \quad \nu \sim \mathcal{N}(0, 1),$$

where γ is a constant, controlling the variance of the random draws. For k=1, we add a fictitious history $\lambda_0=\lambda_1$, where λ_1 is drawn from a normal distribution with zero mean and standard deviation 0.1. The standard deviation of the innovation process is $\gamma=0.08$. The data were corrupted by exogenous scaled white noise with variance $10^{-3} \times \|b_0\|_{\infty}^2$, or standard deviation approximately 3 percent of the maximum entry of the noiseless data.

Figure 4 shows the ensemble mean and the 95% credible intervals calculated by the algorithm with two different profiles. The sinusoidal profile (left) is in line with the smoothness assumptions, and the ensemble mean is following the true profile with reasonable fidelity, with the uncertainty increasing considerably when moving inwards. In the discontinuous case (right), the ensemble mean shows that the smoothness assumptions of the prior are not fully in line with the generative signal, thus it is not surprising that the jumps are not well captured.

6.2. Non-radial conductivity, continuous model

In the second computed example, we generate the synthetic data by the second order FEM approximation with isoparametric elements along the boundary. The mesh, generated with DistMesh [43], consists of 3548 elements and 7369 nodes, with the diameter of the triangles in the center roughly five times the diameter of the triangles on the boundary. The number of sine and cosine current densities applied to the boundary is n/2 = 30, so the Neumann-to-Dirichlet matrix is of size 60×60 . The conductivity profile used for generating the data is shown in the last panel of the figure 5. To estimate the modeling error, we generated a sample of 1000 conductivities with Gaussian inclusions, with random cardinality between one and four, random positions and strictly positive amplitudes, and computed the boundary data with both the FEM model and the first order Möbius solver to generate a sample of realizations of the modeling error. In addition to the estimated modeling error,

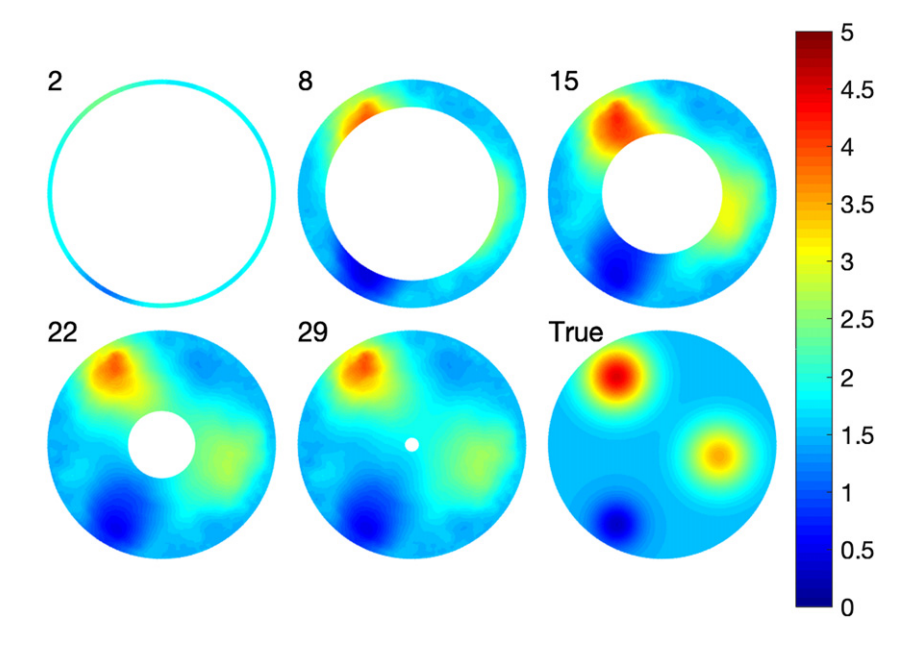


Figure 5. Progression of the conductivity estimates at selected instances of the layer striping process based on the continuous data model. The numbers indicate the current ring, while the last panel shows the generative model used to compute the data. The Neumann-to-Dirichlet matrix was computed by using a finite element approximation.

Gaussian scaled white noise with the variance $10^{-7} \times ||b||_{\infty}^{2}$ was added to the data corresponding to a standard deviation of about 0.3% of the maximum of the absolute value of the data. Observe that at high frequencies, the relative noise level is higher than at low frequencies. The values of the parameters in the prior for generating the conductivity are given in table 2

Figure 5 shows the progression of the ensemble mean for different radial values R_j , as well as the true conductivity that was used to generate the data. The results show an accurate localization of the inhomogeneities, and a good resolution of the dynamical range. In numerical tests with significantly smaller prior variance values (not shown here), the algorithm had some difficulties, which is understandable, since the predictive ensemble may not contain particles able to explain the data.

6.3. Non-radial conductivity, electrode data

Finally, we run the algorithm adapted to the electrode data. The simulated data were computed by using a second order FEM model with 32 uniformly distributed electrodes. For the details of the computational model, we refer to [11]. The contact impedances were assumed to be all equal, $z_{\ell} = 0.01$ and known. The values of the prior parameters were chosen as in the continuous data case. The modeling error covariance was estimated by calculating the electrode data with the finite element CEM model, and comparing it to the resistance matrix obtained by combining the Riccati solver with the mapping (26). The results, shown in figure 6, show that the algorithm performs as well with electrode data as with continuous data.

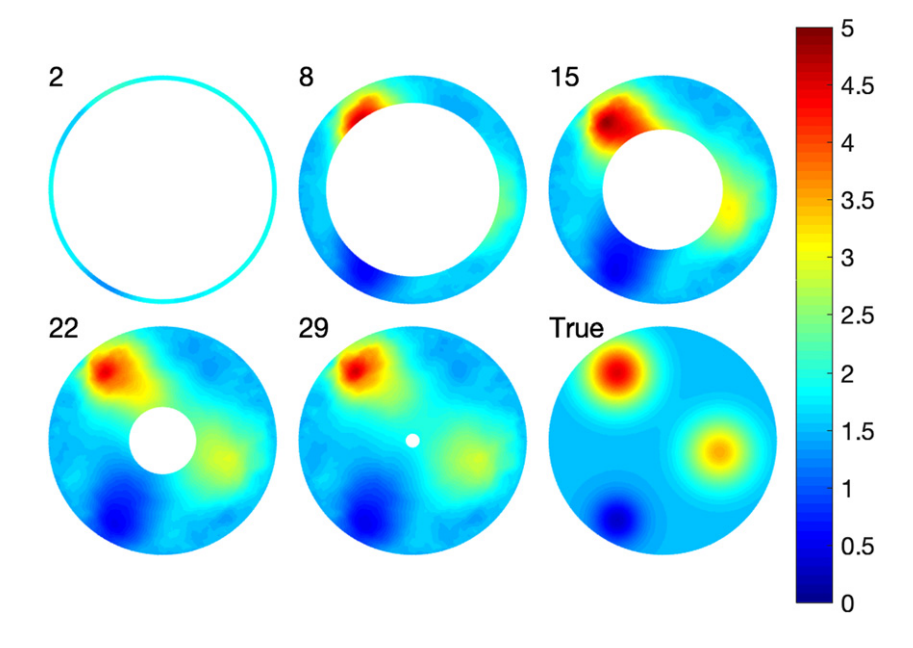


Figure 6. Progression of the conductivity estimates at selected instances of the layer striping process based on the complete electrode model data. The numbers indicate the current ring, while the last panel shows the generative model used to compute the data. The Neumann-to-Dirichlet matrix was computed by using a finite element approximation.

7. Discussion

The layer stripping algorithm in its original formulation suffered from numerical instabilities that limited its performance. To overcome some of the problems, we recast it in the Bayesian framework and proposed a novel numerical algorithm that combines the Möbius forward solver, ensemble Kalman filter and modeling error compensation. Numerical examples illustrate the viability of the proposed algorithm. The implementation of the Bayesian layer stripping algorithm in this article assumes that a noisy observation of the Neumann-to-Dirichlet operator or the resistance matrix is available, and the performance of the approach was demonstrated using computed examples in a disc. From the practical point of view, one can ask whether the approach can be extended to more general domains. While theoretically it is not difficult to extend the approach to any two or three dimensional domain for which a tangent-normal coordinate system is available at least near the boundary, the numerical implementation may pose some challenges. Another question that is of practical importance is the modeling of the noise in the boundary operator which in practice needs to be constructed from noisy current-voltage pairs. In the present article, a simplified additive Gaussian scaled white noise model was used as a proof of concept. We demonstrated that unlike the original layer stripping algorithm, the Bayesian version allows a natural extension to the case in which the data arise from realistic electrode measurements. The testing of the algorithm with real data, including the incorporation of a realistic noise model, will be part of a future research.

Acknowledgments

The work of D C was partly supported by NSF grant DMS-1522334, and of S N and E S by NSF grant DMS-1714617.

ORCID iDs

D Calvetti https://orcid.org/0000-0001-5696-718X E Somersalo https://orcid.org/0000-0001-5099-3512

References

- [1] Arnold A, Calvetti D and Somersalo E 2014 Parameter estimation for stiff deterministic systems via ensemble Kalman filter *Inverse Problems* **30** 105008
- [2] Arridge S R, Kaipio J P, Kolehmainen V, Schweiger M, Somersalo E, Tarvainen T and Vauhkonen M 2006 Approximation errors and model reduction with an application in optical diffusion tomography *Inverse Problems* 22 175–95
- [3] Astala K and Päivärinta L 2006 Calderón's inverse conductivity problem in the plane *Ann. Math.* **163** 265–99
- [4] Bergh J and Löfström J 1976 Interpolation Spaces (Berlin: Springer)
- [5] Brenner S and Scott R 2007 The Mathematical Theory of Finite Element Methods (New York: Springer)
- [6] Brühl M and Hanke M 2000 Numerical implementation of two non-iterative methods locating inclusions in impedance tomography *Inverse Problems* 16 1029–42
- [7] Cakoni F, Colton D and Haddar H 2002 The linear sampling method for anisotropic media J. Comput. Appl. Math. 146 285–99
- [8] Calderón A P 1980 On an inverse boundary value problem Seminar on Numerical Analysis and Its Applications to Continuum Physics (Rio de Janerio: Soc Brasileira de Matematica)
- [9] Calvetti D, Dunlop M, Somersalo E and Stuart A 2018 Iterative updating of model error in Bayesian inversion *Inverse Problems* 34 025008
- [10] Calvetti D, Ernst O and Somersalo E 2014 Dynamic updating of numerical model discrepancy using sequential sampling *Inverse Problems* 30 114019
- [11] Calvetti D, Nakkireddy S and Somersalo E 2019 Approximation of continuous EIT data from electrode measurements with Bayesian methods *Inverse Problems* 35 045012
- [12] Calvetti D and Somersalo E 2007 Bayesian Scientific Computing: Ten Lectures on Subjective Computing (New York: Springer)
- [13] Chada N K, Iglesias M A, Roininen L and Stuart A M 2018 Parameterizations for ensemble Kalman inversion *Inverse Problems* 34 055009
- [14] Cheney M and Kristensson G 1988 Three-dimensional inverse scattering: layer-stripping formulae and ill-posedness results *Inverse Problems* 4 625
- [15] Cheney M and Isaacson D 1992 Invariant embedding, layer-stripping and impedance imaging Invariant Imbedding and Inverse Problems vol 63 (Philadelphia, PA: SIAM) p 42
- [16] Cheng K-S, Isaacson D, Newell J C and Gisser D G 1989 Electrode models for electric current computed tomography IEEE Trans. Biomed. Eng. 3 918–24
- [17] Del Moral P, Doucet A and Jasra A 2006 Sequential Monte Carlo samplers J. Roy. Stat. Soc. B Stat. Methodol. 68 411–36
- [18] Doucet A, Godsill S and Andrieu C 2000 On sequential Monte Carlo sampling methods for Bayesian filtering Stat. Comput. 10 197–208
- [19] Evans L C 2010 Partial Differential Equations 2nd edn (Providence, RI: AMS)
- [20] Evensen G 2009 Data Assimilation: The Ensemble Kalman Filter (Berlin: Springer)
- [21] Gockenbach M S 2006 Understanding and Implementing the Finite Element Method vol 97 (Philadelphia, PA: SIAM)
- [22] Grisvard P 2011 Elliptic Problems in Nonsmooth Domains (Philadelphia, PA: SIAM)

- [23] Hyvönen N 2009 Approximating idealized boundary data of electric impedance tomography by electrode measurements Math. Models Methods Appl. Sci. 19 1185–202
- [24] Hyvönen N 2009 Comparison of idealized and electrode Dirichlet-to-Neumann maps in electric impedance tomography with an application to boundary determination of conductivity *Inverse Problems* 25 085008
- [25] Iglesias M A, Law K J and Stuart A M 2013 Ensemble Kalman methods for inverse problems Inverse Problems 29 045001
- [26] Ikehata M and Siltanen S 2000 Numerical method for finding the convex hull of an inclusion in conductivity from boundary measurements *Inverse Problems* 16 1043–52
- [27] Isaacson D, Mueller J L, Newell J C and Siltanen S 2004 Reconstructions of chest phantoms by the D-bar method for electrical impedance tomography IEEE Trans. Med. Imaging 23 821–8
- [28] Katzfuss M, Stroud J R and Wikle C K 2016 Understanding the ensemble Kalman filter Am. Stat. 70 350-7
- [29] Kaipio J P and Somersalo E 2007 Statistical inverse problems: discretization, model reduction and inverse crimes J. Comput. Appl. Math. 198 493–504
- [30] Kaipio J and Somersalo E 2004 Statistical and Computational Inverse Problems (New York: Springer)
- [31] Kirsch A 2005 The factorization method for a class of inverse elliptic problems *Math. Nachr.* **278** 258–77
- [32] Kohn R and Vogelius M 1984 Determining conductivity by boundary measurements Commun. Pure Appl. Math. 37 289–98
- [33] Majda A J and Harlim J 2012 Filtering Complex Turbulent Systems (Cambridge University Press)
- [34] Nachman A I 1988 Reconstructions from boundary measurements Ann. Math. 128 531-76
- [35] Nachman A I 1996 Global uniqueness for a two-dimensional inverse boundary value problem Ann. Math. 143 71–96
- [36] Nakamura G and Uhlmann G 1997 A layer stripping algorithm in elastic impedance tomography Inverse Problems in Wave Propagation (New York: Springer) pp 375–84
- [37] Roininen L, Huttunen J M and Lasanen S 2014 Whittle-Matérn priors for Bayesian statistical inversion with applications in electrical impedance tomography *Inverse Problems Imaging* 8 561–86
- [38] Schiff J and Shnider S 1999 A natural approach to the numerical integration of Riccati differential equations SIAM J. Numer. Anal. 36 1392–413
- [39] Schillings C and Stuart A M 2017 Analysis of the ensemble Kalman filter for inverse problems SIAM J. Numer. Anal. 55 1264–90
- [40] Somersalo E, Isaacson D, Cheney M and Isaacson E 1991 Layer stripping: a direct numerical method for impedance imaging *Inverse Problems* 7 899–926
- [41] Somersalo E, Isaacson D and Cheney M 1992 Existence and uniqueness for electrode models for electric current computed tomography SIAM J. Appl. Math. 52 1023–40
- [42] Somersalo E 1994 Layer stripping for Maxwell's equations with high frequency *Inverse Problems* **10** 449–66
- [43] Persson P O and Strang G 2004 A simple mesh generator in MATLAB SIAM Rev. 46 329-45
- [44] Sylvester J 1992 A convergent layer stripping algorithm for the radially symmetric impedance tomography problem Commun. PDE 17 1955–94
- [45] Sylvester J, Winebrenner D and Gylys-Colwell F 1996 Layer stripping for the Helmholtz equation SIAM J. Appl. Math. 56 736–54
- [46] Sylvester J and Uhlmann G 1987 A global uniqueness theorem for an inverse boundary value problem Ann. Math. 125 153–69